Evaluation of Ion Temperature and Plasma Rotation at LHD from Charge-Exchange Spectra with Photon-Statistical Weighting[*)]

Bernd WIELAND, Katsumi IDA and Mikirou YOSHINUMA

National Institute for Fusion Science, 322-6 Oroshi-cho, Toki, Gifu 509-5292, Japan

A new diagnostic for LHD is presented, which utilizes active charge-exchange signals from Hydrogen (main ions) and Helium (impurity ions) to derive the radial ion-temperature and ion-velocity profiles as well as the H/He ratio profile. In a sensitivity study, different models for profile fitting and measurement uncertainties are compared, which leads to first results. This covers fitting with one Gauss function and two Gauss functions as well as the inclusion of read-out noise and photon noise. Full error propagation from the measured spectra to the resulting profiles is provided by utilizing Bayesian statistics in combination with a weighted least-squares fit and boundary conditions. Reliable and accurate results were achieved for the ion-temperature profiles, which are in good agreement with the well-proven Carbon diagnostic. Concerning the quality of the velocity profiles, no statement could be made. The H/He ratio measurements in contrary lead to accurate results. Calibration with the H/He ratio of passive emission near the plasma edge just before the end of the discharge allows calculating absolute values for Helium and Hydrogen density profiles.

1. Introduction

At LHD, transport studies and high performance scenario development are of increasing interest. Therefore, exact knowledge of profiles of plasma parameters like temperature, density or rotation velocity is essential in order to compare experimental data to transport models and other theories. Also the exact density ratios of the main ions to the impurity ions are important, because the heating efficiency is dependent on this ratio [1]. Up to now the temperature, density and velocity measurements were done by measuring carbon impurity ions using active charge-exchange spectroscopy. But as it is shown in reference [2], hollow impurity density profiles reduce the accuracy of the measurements in the central region especially for highly confined plasma. In order to overcome the problem of low Carbon signal for ion-temperature measurements, a main ion (Hydrogen) charge-exchange diagnostic was installed at LHD. This paper introduces the charge-exchange spectroscopy system for main ions, presents a model comparison for spectrum fitting and provides a basic model to derive the most important radial profiles in the framework of a sensitivity study: ion-temperature, ion-velocity and H/He ratio.

2. Experimental Setup

The experimental setup for data acquisition is sketched in Fig. 1. The photons from the experiment are transported by 8 optical fibers with a diameter of 200 μm to the diffractive beam splitter. The radial coverage of the fibers is from 3.8 m to 4.7 m of the major radius. The diffractive beam splitter has 16 output channels that are connected to the spectroscope: 8 for observing Hydrogen lines and 8 for observing Helium lines. In order to eliminate the interference with other lines, a band-pass filter has been installed. The spectrometer has a focal length of 400 mm and a f-number of 2.8. To be able to record the spectra of both elements (H and He) simultaneously, two gratings are installed: the one for Hydrogen has a groove density of 1200 lines/mm and a dispersion of 0.019 nm/pixel; the one for Helium has a groove density of 1800 lines/mm and a dispersion of 0.013 nm/pixel. The
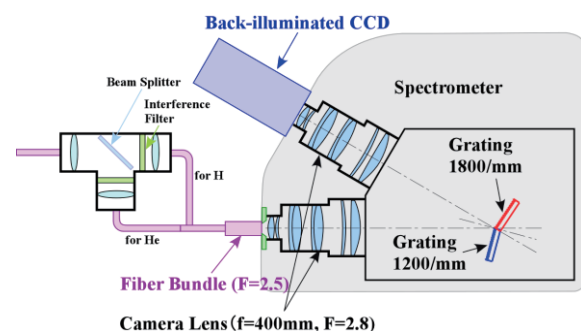
Fig. 1 Sketch of diffractive beam splitter, optics and the spectrometer.

spectra are captured by a frame-transfer CCD camera with 640×480 pixel and a exposure time of 5 ms. The pixel size is 12 µm. This system is designed to measure the active charge-exchange signal with a neutral heating beam (H^0-ions) of singly charged Hydrogen at 656.28 nm and of singly charged Helium at 468.6 nm. The charge-exchange reaction for the plasma main ions is given by:

$$H^0 \, (NBI) \, + H^+ \, (main \, ions) \, \rightarrow H^+ + H^{0*}, \qquad (1)$$
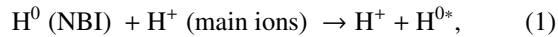
where the observed line is emitted by the neutralized and excited plasma main ions H^{0*}. In the case of Helium, the reaction is given by:

$$H^0(NBI) + He^{2+} \, \rightarrow \, H^+ + He^{+*}, \qquad (2)$$
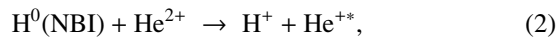
where the main difference is the charge of the excited ions.

3. Data Acquisition

Examples for the raw spectra recorded by the CCD camera are given in Figs. 2 and 3. The spectrum indicated by a black, solid line includes active charge-exchange component and background radiation during NBI injection, while the dashed red spectrum only includes the background signal without beam injection. The background spectrum is an interpolation using the last frame before the beam is switched on and the first frame after it is switched off. In the case of Hydrogen, the main ions, one can clearly identify the beam emission component on the left, the high central peak consisting of the passive edge H_α-line superposed by the active CXS signal and on the right, the emission line of other impurities. In the case of Helium, there are emission lines of other impurities on the left. The feature directly left of the He-line is a leakage of H_α-line radiation in the diffractive beam splitter. The newly installed band-pass interference filters removed this contribution successfully. Background subtraction is utilized to extract the active charge-exchange part of the spectra. The remaining features are the beam emission component, the active CXS signal and possibly the fast-ion contribution for the main ions (Hydrogen) and only the active charge-exchange signal in the case of the impurity-ion species Helium. Concerning the measurement errors, one can estimate the read-out noise to approximately 10 counts, which is dominant in the wings of the spectra. In the area around the maximum, photon statistics is the leading uncertainty. Consequences on the fitting of the spectra and on the resulting radial profiles are discussed in the next section.
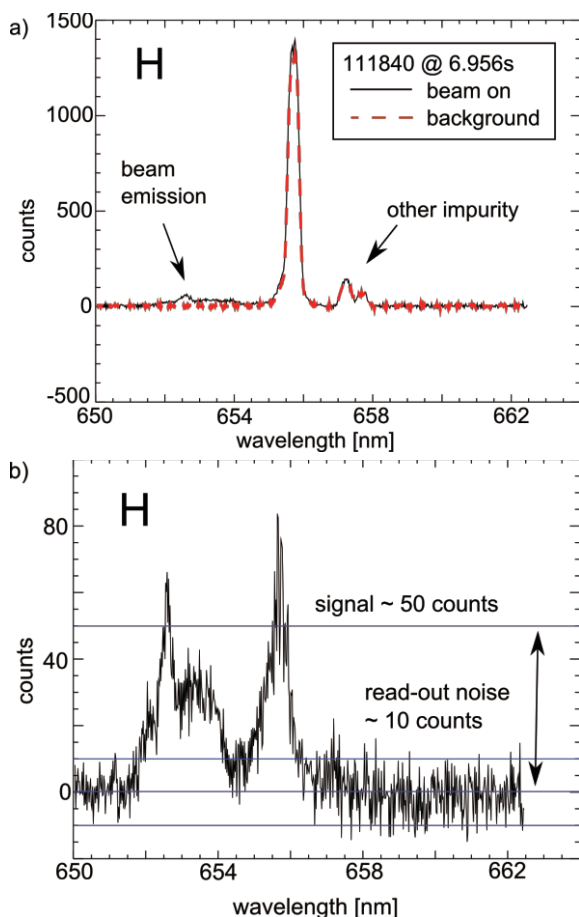
Fig. 2 a): recorded raw data (black, solid) with background frame (red, dashed) for Hydrogen. b): background subtracted spectrum.
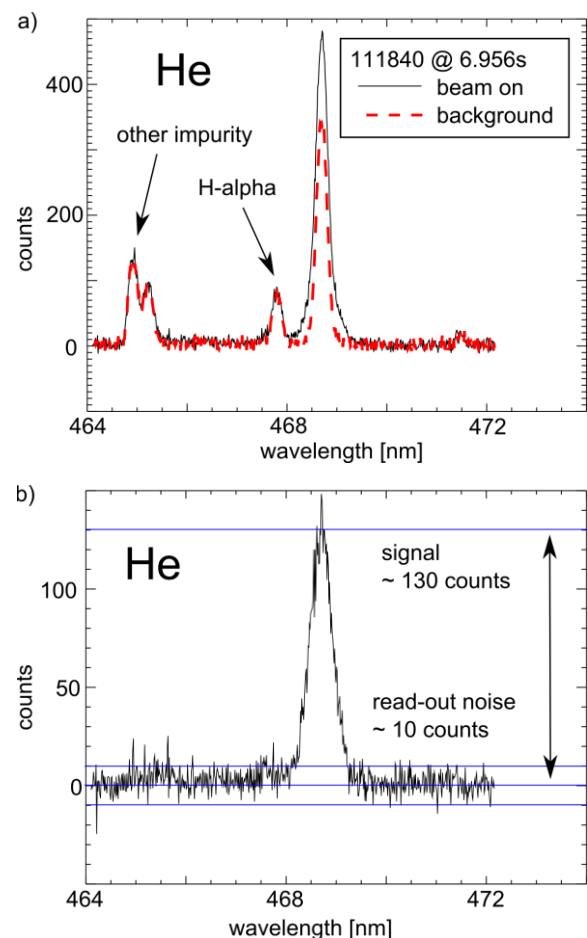

Fig. 3 a): recorded raw data (black, solid) with background frame (red, dashed) for Helium. b): background subtracted spectrum.

4. Model Comparison

In order to derive radial profiles of important plasma parameters like temperature or velocity from the measured spectra, an adequate model of the measured spectrum had to be selected. Two approaches were tested, where the first uses a single Gauss-shape, assuming that the measured spectrum is dominated by one emission line, the active charge-exchange signal. The second one assumes that the observed active charge-exchange line is superposed by additional interfering signals and therefore a double Gaussian fit was used.

Applying background-subtraction and a correction for the spectrometer function gives good results in the case of Helium (see Fig. 4) for the single Gaussian approach. The active charge-exchange line emission is superposed only by a small passive component from the edge, that is removed by background-subtraction. In the case of Hydrogen, things are different. There is a very strong passive
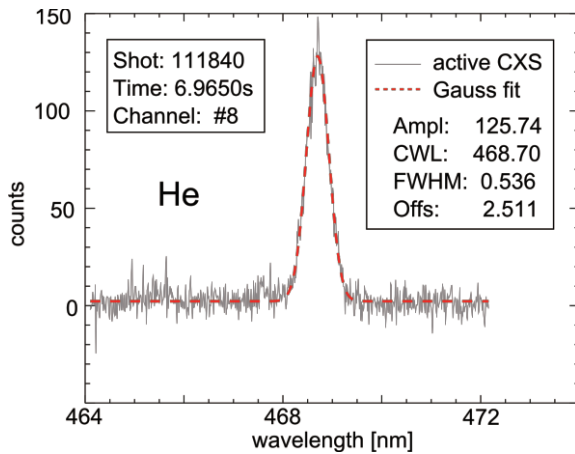

Fig. 4 Fit of the background subtracted He spectrum with a single Gauss approach.
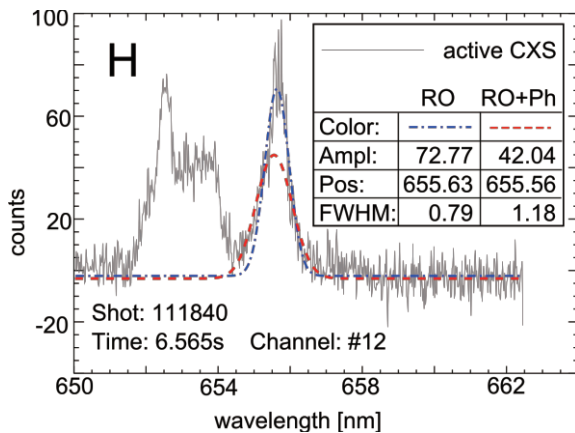
Fig. 5 Comparison of two different approaches of determining the error of the measured spectra. In the blue dash dot fit, only read-out noise is taken into account while in the red dashed fit, read-out noise and photon statistics is considered.

H_α-line superposed by a small active charge-exchange signal. Background-subtraction is not accurate enough to remove the strong background completely. In order to still get reliable fitting results, a more advanced assumption for the measurement error was implemented. In Fig. 5, the fitting results for read-out noise only and read-out noise combined with photon statistics are compared. The error assumption for the blue dash dotted fit is solely based on read-out noise:

$$\sigma_{d_A} = \sigma_{d_B} = \sigma_{RO} \tag{3}$$

$$d = d_A - d_B \rightarrow \sigma_d = \sqrt{\sigma_{d_A}^2 + \sigma_{d_B}^2} = \sqrt{2} \cdot \sigma_{RO} \tag{4}$$

d_A represents the measured data during NBI heating, thus the active signal is present, whereas d_B represents the background frame. The read-out noise is given by σ_{RO}. The background subtracted spectrum and its uncertainty is specified by d and σ_d.

The more advanced error assumption (dashed red), which takes photon statistics into account is implemented in the following way:

$$\sigma_{d_A} = \sqrt{\frac{d_A}{\gamma} + \sigma_{RO}^2}, \tag{5}$$

where γ is the count-to-photon conversion factor. For a high number N of counted photons, the statistical error can be derived from the Poisson distribution and is given by $\sqrt{N}$ [3]. Also in this case, background subtraction is used and the error of the fitted spectra is given by:

$$\sigma_d = \sqrt{\sigma_{d_A}^2 + \sigma_{d_B}^2} \approx \sqrt{2} \cdot \sigma_{d_A} = \sqrt{2} \cdot \sqrt{\frac{d_A}{\gamma} + \sigma_{RO}^2} \tag{6}$$

The conversion factor γ has been determined from the local variation of the measured data. An exact measurement of this factor is planned at the end of this year's campaign.

As a result of photon-statistical weighting, the wings of the Hydrogen spectrum, which mainly carry the active charge-exchange information are weighted higher than the central region, which is disturbed severely by the strong passive edge radiation. Therefore, the estimated width represents the active charge-exchange component much better than the read-out noise only approach, which is governed by the stronger passive edge radiation.

The second approach to fit the spectra was realized by using a double Gaussian fit. The basic idea behind this is the non-perfect removal of the passive edge emission by background subtraction. Therefore, in a first step, the background spectrum is fitted by a single Gaussian to get an estimate of the position and the width of the passive edge emission. In a second step, the background subtracted spectrum is fitted by two Gauss functions, a hot component for the active charge-exchange signal and a cold component for the remains of the background. The cold component is restricted by the position and width estimated in the
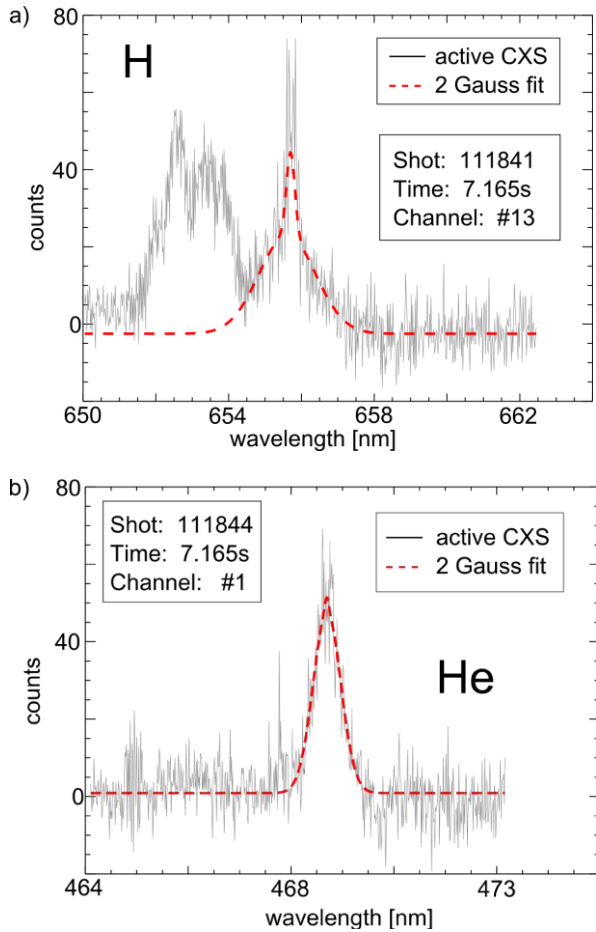
Fig. 6 The background subtracted spectra are fitted by two Gauss functions. a): Hydrogen spectrum. b): Helium spectrum.

first step. Like in the single Gaussian approach, full error propagation is used, covering read-out noise and photon statistics. Examples for the results for Hydrogen and Helium are given in Fig. 6.

5. Fitting of the Spectra

The fitting algorithm itself is implemented as a weighted least-squares minimization with boundary conditions. The squared residuals are given by

$$\chi^2 = \sum_j \left(\frac{d_j - r_j}{\sigma_{d_j}}\right)^2,$$ (7)

where d_j is a single point of a measured spectrum and r_j the output of the fit for this point. σ_{d_j} is the associated measurement error. The origin of least-squares fitting is a simplification (maximum likelihood estimate) of Bayesian statistics, where probability is utilized as a measure for the truth of a hypothesis [3]. A probability density function (PDF) is used to express the agreement of the model $M(x)$ and the chosen set of parameters x with the measured data d and the available background information I: $p(M(x)|d, I)$ (posterior PDF). The model parameters which

maximize this function are the best possible fit taking all given information into account. For parameter estimation problems the posterior PDF is given as the product of the likelihood PDF $p(d|M(x), I)$ and the prior PDF $p(M(x)|I)$, where the likelihood is a measure of the likeliness of reproducing the measured data, using a given set of model parameters [3]. The prior PDF is a measure of how well this set of parameters agrees with additional information like boundary conditions. In the case where only read-out noise is taken into account, the prior PDF is flat and all uncertainties are equal $\sigma_{d_j} = \sigma_{RO}$. This results in a standard least-squares fit, which maximizes the likelihood PDF. Including photon statistics requires a weighted least-squares fit, because the measurement error at each point of the spectra differs and the residuals are defined like in equation (7):

$$p(M(x)|d, I) \propto p(d|M(x), I) \propto \exp\left(-\frac{\chi^2}{2}\right)$$ (8)

If boundary conditions are added like it is the case for the double Gaussian fit, the prior PDF cannot be neglected any more. An uncertain set-value $x_{0,i} \pm \sigma_{x_{0,i}}$ for a specific parameter i leads to the following contribution to the prior PDF:

$$\chi_{p,i}^2 = \left(\frac{x_i - x_{0,i}}{\sigma_{x_{0,i}}}\right)^2,$$ (9)

$$p_i(M(x)|I) \propto \exp\left(-\frac{x_{p,i}^2}{2}\right).$$ (10)

Being statistically independent, these probabilities have to be multiplied and the posterior PDF is given by:

$$p(M(x)|d, I) \propto \exp\left(-\frac{\chi^2}{2}\right) \cdot \prod_i \exp\left(-\frac{\chi_{p,i}^2}{2}\right),$$ (11)

which can be simplified to:

$$p(M(x)|d, I) \propto \exp\left(-\frac{\chi_S^2}{2}\right) \quad \text{with}$$

$$\chi_S^2 = \chi^2 + \sum_i \chi_{p,i}^2.$$ (12)

The minimum of χ_S^2 is determined using the Powell's method from the Numerical Recipes in Fortran 77 [5]. The uncertainties of the estimated parameters were calculated, based on the curvature of the posterior PDF at the maximum as described in [3]. A practical application of this method can be found for example in [4]. The logarithm $L = \log p(M(x)|d, I)$ of the posterior PDF is expanded in a Tailor series at the maximum, where the quadratic term is dominant. Neglecting all higher terms lead to an approximation of the posterior PDF by a Gaussian function. The width of this symmetric normal distribution is then given by

$$\sigma_{x,i} = \left(-\frac{d^2L}{dx_i^2}\Big|_{x_i}\right)^{-1/2}.$$ (13)

The uncertainty $\sigma_{x,i}$ of the estimated parameter x_i is large, if the posterior PDF has a flat maximum and small, if it has a peaked maximum quantified by one over the square root of the second derivative of the posterior PDF.

6. Profile Calculation

Having estimated the model parameters together with their uncertainties, it was possible to calculate the radial ion-temperature profile, the radial ion-velocity profile and a radial profile of the Hydrogen to Helium ratio. The hot component, which models the active charge-exchange signal, is given by

$$f(\lambda) = A \cdot \exp\left(-\frac{(\lambda - \lambda_c)^2}{2w^2}\right), \tag{14}$$

where A is the amplitude, λ_c is the central wavelength and w the width of the emission line.

For the calculation of the temperature profile, the width w is the important parameter. It is connected to the temperature by Doppler-broadening:

$$w = \frac{\lambda}{c}\sqrt{\frac{k \cdot T}{m}}. \tag{15}$$

Solving this equation for the temperature leads to

$$T\,[\text{eV}] = \left(\frac{w_{\text{corr}}}{\lambda_c} \cdot c\left[\frac{\text{m}}{\text{s}}\right]\right)^2 \cdot \frac{m\,[\text{u}] \cdot u\,[\text{kg}]}{k_B\left[\frac{\text{J}}{\text{eV}}\right]}, \tag{16}$$

with an uncertainty of

$$\sigma_T = T\,(w_{\text{corr}}, \lambda_c) \cdot \sqrt{\left(\frac{2\sigma_{w_{\text{corr}}}}{w_{\text{corr}}}\right)^2 + \left(\frac{2\sigma_{\lambda_c}}{\lambda_c}\right)^2}, \tag{17}$$

by using Gaussian error propagation. In these equations, w_{corr} is the width corrected for the spectrometer function, m the atomic mass, u the atomic mass unit, c the speed of light and k_B the Boltzmann constant.

The central wavelength is important in order to derive the velocity profile from the Doppler shift of the emission line:

$$\lambda_c = \lambda_0\left(1 - \frac{v}{c}\right), \tag{18}$$

which leads to the following implementation

$$v = c \cdot \left(1 - \frac{\lambda_c}{\lambda_0}\right) \tag{19}$$

and uncertainties:

$$\sigma_v = c\frac{\lambda_c}{\lambda_0}\sqrt{\left(\frac{\sigma_{\lambda_c}}{\lambda_c}\right)^2 + \left(\frac{\sigma_{\lambda_0}}{\lambda_0}\right)^2}. \tag{20}$$

In order to calculate the Hydrogen to Helium ratio, the intensity I for both types of ions is necessary. They were calculated by determining the area enclosed by the fitted line profile for both species:

$$I = \sum_i f(\lambda_i). \tag{21}$$

Dividing these values of H and He at the same radial po-

sition by each other, results in a relative ratio profile. This works even without absolute intensity calibration, because they origin from the same line of sight, separated only by the diffractive beam splitter and they are analyzed with the same spectrometer.

7. Results

The actual concept of the data analysis has been developed as a feasibility study in order to decide, if ion-temperature, ion-velocity and H/He ratio profiles can be determined in a reliable way using main ion (Hydrogen) spectroscopy. Therefore, only a small sub-set of potentially important physical effects are implemented so far. The spectrum is separated in a hot component from active charge-exchange and in a cold component that is given by the remains of the passive signal from the edge after background subtraction. Also the broadening effect of the entrance slit of the spectrometer is taken into account. However, the asymmetric modifications of the H_α spectrum by the fast-ion contribution [7] as well as effects due to the beam HALO [6] and "plume"-effect [6] are neglected.

The rotation velocity for the analyzed discharges is very low and radial variation is in the same order of magnitude than the estimated uncertainties. This is in agreement with the results from velocity profiles provided by the Carbon diagnostic [8] used for cross-validation. Figure 7 b) shows a typical velocity profile of the analyzed discharges. The results based on Helium spectra have a much higher accuracy than the results from Hydrogen spectra, because there is a large amount of Helium in this discharge (H/He-ratio ~0.6). Furthermore, in the case of Hydrogen, the central region of the spectrum is disturbed by the remains of the edge H_α-line. For the analyzed data, no absolute wavelength calibration was available, which allows only relative profiles to the channel with the strongest signal ($R = 4.25$ m). In Fig. 7 b), the results from Carbon are shifted in order to also be relative to this channel.

Very accurate and reliable results were achieved for the ion-temperature profile for both ion types. Good agreement was found with the Carbon measurements (see Fig. 7 a)). Reasons for this are the accurately measured wings of the Helium and Hydrogen spectra defining the width of the fitted spectrum. The good agreement of the Hydrogen results for this type of discharges, despite of the basic model and the different physical behavior of the excited species (singly charged Helium, neutral Hydrogen), needs to be investigated in more detail in the actual 2012 campaign.

In Fig. 7 c), two different H/He ratio profiles are presented, one of them is a discharge with a feedback controlled high amount of Helium (111840) and the other one with a lower amount (111863). Even though there was no absolute intensity calibration, these ratios could be calculated because the light from the same LOS is used and therefore the calibration factor cancels out. Subsequent
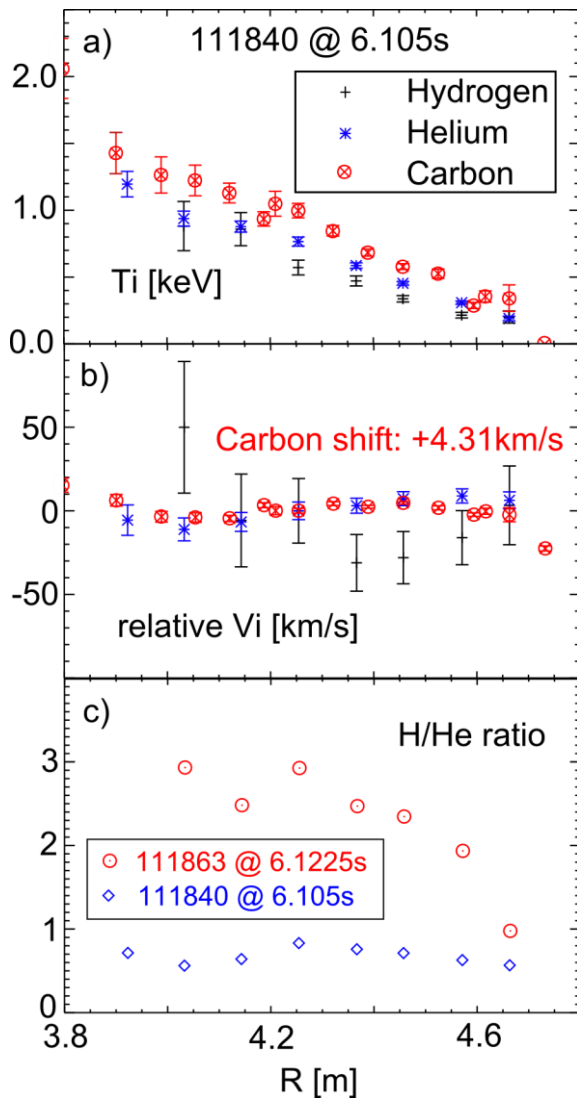
Fig. 7 a), b): Comparison of profiles for H and He cross-checked with profiles from the Carbon diagnostic. c): H/He ratios for discharges with different feedback regulated amounts of Helium.

calibration using the H/He ratio of passive emission near the plasma edge just before the end of the discharge, which can be modeled by collisional-radiative theory, allows to derive absolute values for the Hydrogen and Helium density profiles [1].

8. Conclusions

In this paper a new diagnostic at LHD is introduced. Active charge-exchange spectroscopy on a heating beam is used to measure simultaneously ion-temperature and ion-velocity of the main ions (Hydrogen) and one impurity species (Helium) utilizing a diffractive beam splitter in combination with a two-grid spectrometer. In the framework of a feasibility study, two different approaches to model the spectra (fitting with one Gauss function and fitting with two Gauss functions) in combination with two different methods for the measurement uncertainties (only

read-out noise as well as read-out noise combined with photon noise) were analyzed. Read-out noise and photon noise in combination with a double Gaussian fit leads to the best results, because it also takes the remains of the passive edge emission into account, which are partly filtered-out by beam modulation combined with background subtraction. Weighted least-squares fitting with boundary conditions is used to optimize the model parameters leading to amplitude, position and width of the active CXS component. The Uncertainties are fully propagated through the applied model by using Bayesian statistics. The curvature at the maximum of the posterior probability density function is used as a measure for the uncertainty of the fit-result. The radial temperature and velocity profiles are calculated utilizing Doppler-broadening and Doppler-shift. The integral of the fitted spectrum is also used to derive H/He ratio profiles. For this feasibility study, advanced effects like the fast ion contribution to the Hydrogen spectrum and the beam HALO are neglected.

Accurate and reliable results could be achieved in the case of the ion-temperature for both species, which are in good agreement with the results from the Carbon charge-exchange diagnostic, used for cross-validation. Also the calculations of the radial H/He ratio profiles give good results. In the case of the velocity profile, the analyzed discharges provide too less radial variation and also a too low overall rotation to make distinct statements.

Having accomplished very promising results in this feasibility study, detailed measurements on a wide variety of discharges in combination with improved hardware are carried out in the on-going campaign. It is planned to explore whether a more complex model leads to improved accuracy. Furthermore, discharges with higher rotation velocity will be analyzed to be able to validate the results by comparing them to the Carbon measurements. Another promising approach that will be explored is to utilize the absolute calibrated H/He ratios at the plasma edge by Goto *et al.* [1] in order to extend the results over the complete measurement region to the plasma center. Concerning the differences between Helium transport and bulk ion transport as well as for optimizing the heating efficiency in the ICRF heating, this is very useful information.

[1] M. Goto and S. Morita, Phys. Plasmas **10**, 1402 (2003).
[2] K. Ida *et al.*, Phys. Plasmas **16**, 056111 (2009).
[3] D.S. Sivia, *Data Analysis: A Bayesian Tutorial* (Oxford University Press, USA; 2. edition, 2006) p.20 ff.
[4] S.K. Rathgeber *et al.*, Plasma Phys. Control. Fusion **52**, 095008 (2010).
[5] W.H. Press, B.P. Flannery, S.A. Teukolsky and W.T. Vetterling, *Numerical Recipes in Fortran 77* (Cambridge University Press, 2. edition, 1992) p.406 ff.
[6] R.C. Isler, Plasma Phys. Control. Fusion **36**, 171 (1994).
[7] B. Geiger *et al.*, Plasma Phys. Control. Fusion **53**, 065010 (2011).
[8] K. Ida, S. Kado and Y. Liang, Rev. Sci. Instrum. **71**, 2360 (2000).